International Journal of Advanced Engineering Research and Science (IJAERS)
Peer-Reviewed Journal
ISSN: 2349-6495(P) | 2456-1908(O)
Vol-13, Issue-3; Mar, 2026
Journal Home Page Available: https://ijaers.com/
Article DOI: https://dx.doi.org/10.22161/ijaers.133.6

Design of a Cross-Counter Flow Channel Architecture using Serpentine Topology

Guan-Hong Xie, Yan-Zuo Chang*, Qi-Hong Tang, Jing-Xin Ou, Zi-Rui He, Jie-Zhen Yang, Kai-Ming Chen, Yu-Xuan Chen, Hong-Rui Yang, Yong-Qing Wang

School of Energy and Power Engineering, Guangdong University of Petrochemical Technology, Maoming, Guangdong 525000, China
*Corresponding Author : 1595709663@qq.com

School of Energy and Power Engineering, Guangdong University of Petrochemical Technology, Maoming, Guangdong 525000, China (Corresponding author: Yan-Zuo Chang), Email: 3435059931@qq.com

Received: 20 Feb 2026,

Received in revised form: 21 Mar 2026,

Accepted: 25 Mar 2026,

Available online: 31 Mar 2026

***Keywords*— ORC, Piston Expander, CFD, Internal Flow Field Characteristics, Clearance Height**

***Abstract*—** *Aiming at the problems of complex internal flow fields and the significant impact of clearance height on performance in Organic Rankine Cycle (ORC) waste heat recovery systems, this paper conducted a 3D steady-state numerical simulation study. Selecting the key working phase where the intake valve is fully open, a refined 3D model covering the intake port and the internal fluid domain of the cylinder was established, and ANSYS Fluent software was used for flow field analysis. The research results show that the computational model constructed in this paper has good convergence; after 5500 iterations, the energy residual reached the* 10^{-7} *level, and the residual curves of various physical quantities tended to be stable. This paper reveals the flow loss mechanism of the key phase of the expander, verifies the effectiveness of steady-state numerical simulation in evaluating the in-cylinder flow field characteristics, and provides theoretical support for further optimizing the intake structure and clearance height.*

I. INTRODUCTION

Driven by the deep adjustment of global energy structure and the increasingly severe protection of ecological environment, Energy saving and emission reduction has become the core orientation of industrial development and technological innovation in the world.China has clearly put forward the " 3060 " dual-carbon strategic objectives, green and low-carbon development to the national top design level, We will promote all-round transformation and upgrading in the areas of energy production, consumption and transportation.In this strategic context, China's electric vehicle industry is showing explosive growth trend, New energy electric vehicles with low energy consumption, zero emissions, high intelligence and other significant advantages, and gradually replace the traditional fuel vehicles, Become the automotive industry transformation and upgrading, help to achieve the goal of the key carrier and core development direction [1-2] .With the continuous expansion of market demand and the acceleration of technology iteration, electric vehicles are evolving rapidly in the direction of high endurance, high power and high fast charging rate. As the core power source of electric vehicle, the energy density and fast charging power of power battery continue to rise.High energy density and high rate charge-discharge technology can significantly improve the overall performance of the vehicle, It also leads to a sharp increase in the heat production rate and total heat production under extreme operating conditions, and the thermal management system is facing unprecedented technical challenges. Studies have shown that the operating temperature of power Li-ion battery pack directly determines its electrochemical

performance, charge-discharge efficiency, cycle life and operation safety. The optimum operating temperature range is 20 ℃ ~ 45 ℃ [3-5] , and the temperature difference in the battery module should not be greater than 5 ℃ [6]. Efficient and reliable thermal management system has become the core technical support to ensure the safe, stable and long-life operation of electric vehicles [7].

The core of thermal management of Li-ion battery pack is to control the cell temperature, reduce the module temperature difference and eliminate the local overheating. The heat dissipation effect directly determines the reliability of the battery system.At present, the main cooling methods include air cooling [8], liquid cooling [9], phase change material cooling [10-11], heat pipe cooling [12], Each has its advantages and disadvantages.The air cooling system has simple structure and low cost, and is widely used in the early low power vehicles, but it has low heat transfer coefficient and limited heat dissipation capacity. It is difficult to adapt high power battery, and the temperature is out of control under high rate condition.

Phase change materials can achieve efficient and uniform temperature cooling passively, with small temperature fluctuations, but they have low thermal conductivity, are prone to softening and leakage, are expensive, and have low space utilization, limiting large-scale applications.Heat pipe cooling has low thermal resistance, fast response, and good temperature uniformity, which can quickly dissipate local heat. However, it has a complex structure, inflexible layout, high cost, and is difficult to adapt to compact power battery packs.Overall, liquid cold plate systems have high heat dissipation efficiency, flexible layout, strong adaptability, and can precisely control temperature and temperature difference. They have become the mainstream design solution for high-power battery thermal management and are also the core focus of this study.

The channel form of liquid cooling directly determines fluid flow, pressure loss, and heat transfer uniformity. The serpentine channel [13] is one of the two most representative structures in engineering. The serpentine channel has a compact structure and sufficient heat transfer, making it suitable for space-constrained scenarios.Existing studies mostly focus on reducing the maximum battery temperature and improving heat dissipation efficiency, taking the reduction in maximum temperature as the core evaluation index for heat dissipation performance.There are also methods to improve the thermal performance of power batteries by adding fins in the channels and changing the channel distribution [14]; however, in practical applications, the uniformity of the flow channel temperature and the ability to suppress local hotspots are equally critical. Local overheating can accelerate battery aging and trigger thermal runaway, and evaluating performance solely based on temperature reduction has obvious limitations.Although traditional serpentine channels provide sufficient heat exchange, the fluid temperature rises significantly along the path, resulting in large temperature differences at the end and poor temperature uniformity, making it difficult to meet the high consistency and high safety thermal management requirements of power batteries.

To address the technical issues of poor temperature uniformity and localized overheating in traditional serpentine channels, and to overcome the limitations of synergistically optimizing heat dissipation efficiency and temperature uniformity, this paper takes the traditional serpentine channel and its improved cross-counter flow channel as research objects, and uses numerical thermal simulation methods to investigate the differences in temperature fields, flow characteristics, and heat transfer performance of the two channels under different coolant inlet velocities.Focus on analyzing the advantages of cross-counter flow channels in improving temperature uniformity and suppressing local overheating, and clarify their technical superiority and engineering value.The research results can provide a reliable theoretical basis for the optimal design, performance evaluation, and engineering selection of liquid cooling channels in power batteries under low flow conditions, and have important theoretical and engineering significance for promoting the development of thermal management technology for power batteries.

II. CONSTRUCTION OF A PHYSICAL MODEL BASED ON A SERPENTINE CROSS-FLOW CHANNEL ARCHITECTURE

The power lithium-ion battery pack is composed of five layers of cells. The battery used in this experiment has a volume of 734.4 cm^3, a coolant density of 1000 ρ/(kg/m^3), a specific heat capacity of 4182 cp/J/(kg·K), a thermal conductivity of 0.538 λ/W/(m·K), and dimensions of 118 mm × 63 mm × 10 mm. The structure is shown in Figure 1. The liquid cooling plates with a cross-counter flow channel are placed on both sides of each cell layer, and the thickness of the liquid cooling plates is 4 mm.The coolant flows in from the inlet, absorbs heat through a simulated cross-counter flow channel, and then converges at the outlet to flow out.The runner is a square runner, with inlet and outlet dimensions of 6mm × 2mm.

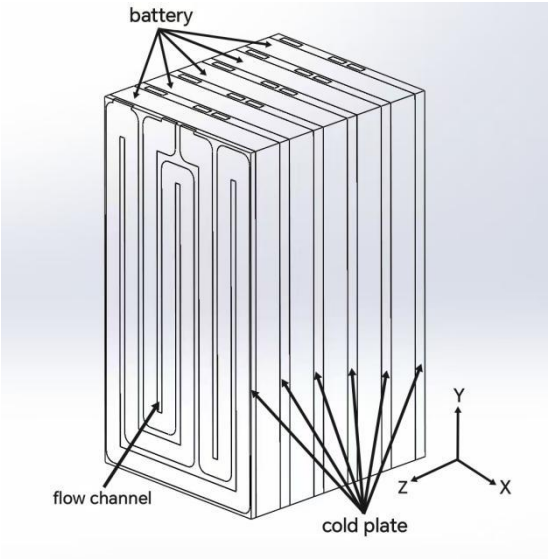

Fig.1: Schematic diagram of cross-counter flow channel geometry

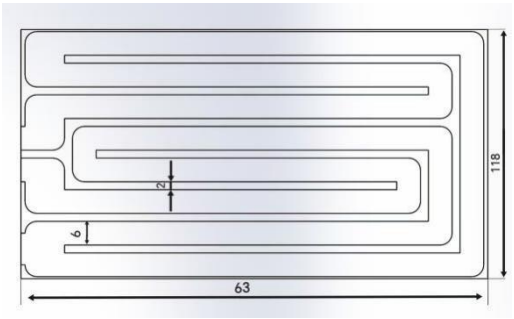

Fig.2: Plan schematic diagram of cross-counter flow channel geometry

III. NUMERICAL MODELS

3.1 Heat Transfer Model

This experiment assumes that the specific heat capacity and thermal conductivity of the battery do not change with temperature; the battery is composed of isotropic and uniformly distributed materials. The heat conduction governing equation for a square lithium-ion battery is:

$$\rho_a C_{pa} \frac{\partial \theta}{\partial t} = \lambda_x \frac{\partial^2 T}{\partial x^2} + \lambda_y \frac{\partial^2 T}{\partial y^2} + \lambda_z \frac{\partial^2 T}{\partial z^2} + q \quad (1)$$

Here, ρ_a, C_{pa}, and q are the battery's average density, specific heat capacity, and heat generation rate, respectively; T is the battery's thermodynamic temperature; λ_x, λ_y, and λ_z represent the thermal conductivities along the x-axis, y-axis, and z-axis, respectively.

The expression for heat generation rate q[15] is as follows:

$$q = \frac{I}{V}(U_0 - U_1) - IT\frac{dU_0}{dT}\frac{1}{V} = \frac{1}{V}\left[IR_t - T\frac{dU_0}{dT}\right] \quad (2)$$

v, I, U_0 and U_1 represent the volume of the single cell, the charging and discharging current, the battery open circuit voltage and the battery end voltage dU0dT are the voltage temperature coefficients, respectively. T is the initial temperature of the battery; Rt is the total resistance of the battery.

The cold plate heat transfer control equation is:

$$\rho_s C_p \frac{\partial^2 T}{\partial t^2} = k_s \left(\frac{\partial^2 T}{\partial x^2} + \frac{\partial^2 T}{\partial y^2} + \frac{\partial^2 T}{\partial z^2}\right) \quad (3)$$

In the formula, ks, T and ρ_s are the heat transfer coefficient, thermodynamic temperature and density of the cold plate, respectively. C_p and T are cold plate density and time, respectively.

In the formula, ks, T, and ρ_s represent the heat transfer coefficient of the cold plate, thermodynamic temperature, and density, respectively; C_p and t represent the density of the cold plate and time, respectively.

3.2 Governing Equations

Continuity Equation:

$$\nabla \cdot \vec{v}_e = 0 \quad (4)$$

Momentum Equation:

$$\frac{\partial(\vec{v}_c)}{\partial t} + (\vec{v}_c \cdot \nabla)\vec{v}_c = -\frac{1}{\rho_c}\nabla \cdot P + \nabla \cdot (u_c \nabla \vec{v}_c) \quad (5)$$

Energy Equation:

$$\frac{\partial(\rho_c T_c)}{\partial t} + \nabla \cdot (\rho_c T_c \vec{v}_c) = \nabla \cdot (k_c \nabla T_c) \quad (6)$$

Where: ρ_c is the density of the coolant; $\vec{v}_c$ and u_c are the velocity vectors of the coolant; C_p is the specific heat capacity of the coolant; Tc is the temperature of the coolant; kc is the thermal conductivity of the coolant.

3.3 Temperature Uniformity Coefficient

The calculation formula is as follows:

$$\Delta T_u = \frac{\sum_{i=1}^{n}(T_{i\max} - T_{i\min})}{n} \quad (7)$$

Where: T_{imax} is the maximum temperature under the given operating condition, T_{imin} is the minimum temperature under the given operating condition, and n is the number of samples.

3.4 Simulation Condition Settings

The flow rates for this experiment were set at 0.3 m/s, 0.4 m/s, 0.5 m/s, 0.6 m/s, and 0.7 m/s, respectively. The channel outlet is a pressure outlet, with the coolant inlet temperature and ambient temperature both at 293.15 K, and the outlet return temperature equal to the ambient temperature. The flow rate is the flow velocity multiplied by 0.24 square centimeters, and the heat source power is 300,000 watts per cubic meter. The inlet temperature is 10°C.

3.5 Grid Independence Test

Mesh independence verification was conducted in the numerical simulation calculations. The maximum and minimum temperatures of the lithium battery pack during the mesh verification are shown in Figure 4.

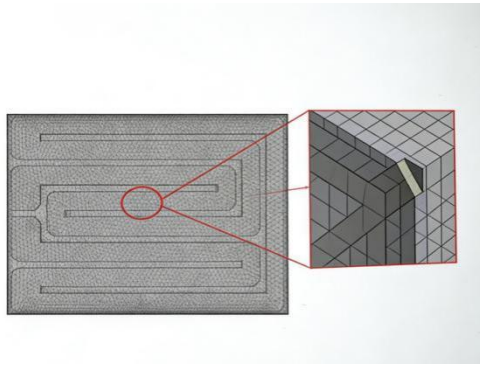

Fig.3: Grid distribution of cross-counter flow channel

For the two types of flow channels, a working condition of 0.3 m/s was used, and calculations were performed with mesh counts of 99,855, 199,710, 399,420, and 798,840 elements, respectively. As shown in Figure 1, after the mesh count reached 399,420, further increasing the number of mesh elements caused almost no change in the maximum and minimum temperatures of the lithium battery pack. Therefore, a mesh count of 399,420 elements was used for the calculations.

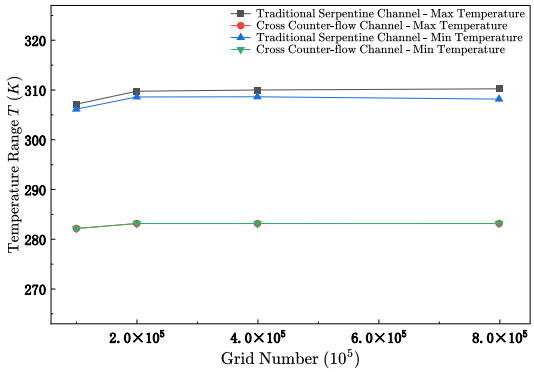

Fig.4: Grid independence test

IV. SIMULATION RESULTS ANALYSIS

4.1 Simulation Results of the Two Flow Channels

This study conducts flow field–temperature field coupled simulations on both traditional serpentine flow channels and cross-counter flow channels, and analyzes the simulation results. Figures 5 and 6 show the temperature cloud maps of the two liquid cooling plates under a flow condition of 0.3 m/s.

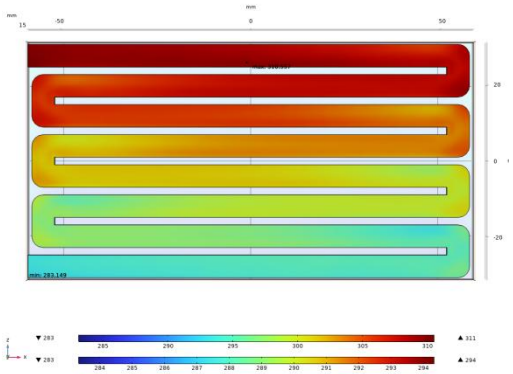

Fig.5: Temperature distribution of conventional serpentine flow channel

As shown in Figure 5, the temperature distribution cloud map of the traditional serpentine flow channel under the condition of 0.3 m/s is illustrated. The flow channel has a long flow path, resulting in significant differences in fluid residence time and heat transfer intensity across various sections. When the fluid first enters, its temperature is 283 K, and the heat transfer efficiency is high; however, by the time the fluid reaches the end, it has absorbed a large amount of heat, causing a substantial decline in the heat transfer capability at the channel's end. At this location, the battery temperature rises to 310 K, forming a 'heat transfer dead zone' and becoming a local hot spot.

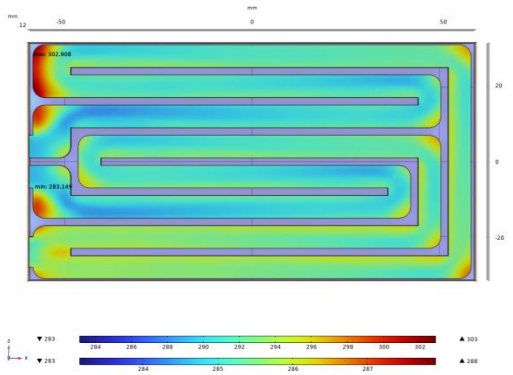

Fig.6: Temperature distribution diagram of cross-counter flow channel

As shown in Figure 6, the temperature distribution cloud map of the cross-counter flow channel under the operating condition of 0.3 m/s indicates that the cross-structure design divides the fluid into two sub channels, shortening the length of a single flow path and reducing the residence time of the fluid in the heat exchange area. The counter flow arrangement reduces the heat exchange temperature difference between the hot and cold fluids to 21 K, while the maximum temperature of the battery decreases to 304 K, maintaining a high degree of temperature uniformity throughout the channel, suppressing local overheating, and

thereby ensuring the consistency of the temperature distribution.

4.1.1 Analysis of Temperature Uniformity

The temperature difference is an important indicator for measuring the temperature uniformity of a liquid cooling plate, and the temperature uniformity of the liquid cooling plate, along with its resistance to local overheating, are key metrics that determine its thermal performance ceiling, system reliability, and device lifespan. The better the temperature uniformity and the weaker the local overheating, the higher the overall heat dissipation efficiency, the lower the thermal resistance, and the more stable the system. The temperature differences of the two types of channels at different flow rates are shown in Figure 7.

Fig. 7 shows the temperature difference R_T of the traditional serpentine and cross counter flow channels with flow velocity v. It can be seen that as the flow rate increases from 0.2m/s to 0.7m/s, the temperature difference of the two runners is downward.

(1) The serpentine flow channel $R_{T,S}$ decreased from 27.0 K to 24.3 K, a decrease of approximately 9.9%;

(2) The cross-counter flow channel $R_{T,C}$ decreased from 19.8 K to 16.8 K, a decrease of approximately 15.2%.

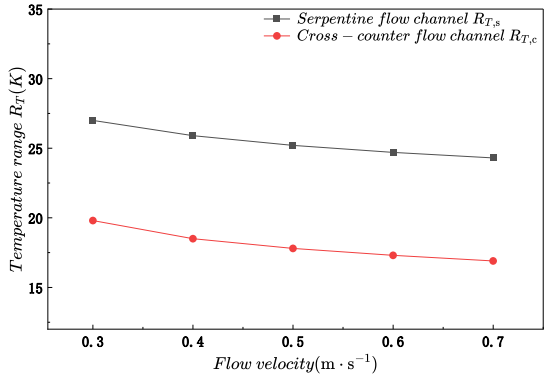

Fig.7: Temperature range of the two flow channels

This indicates that an increase in flow velocity can improve overall temperature uniformity. The cross-counter flow channel shows a more significant response to changes in flow velocity, suggesting that its flow field and temperature field achieve better synergistic optimization.

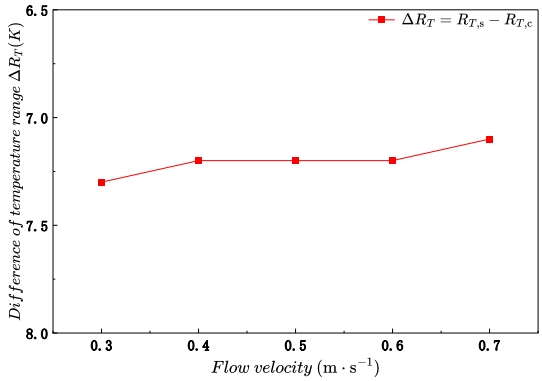

Fig.8: Difference in temperature range between the two flow channels

Figure 8 shows the variation of the difference $\Delta R_T = R_{T,S} - R_{T,K}$ in the maximum temperature difference between the two types of flow channels with flow rate. It can be seen that ΔR_T remains basically stable between 7.1 and 7.2 K. This indicates that the temperature uniformity of the cross-counter flow channel is superior to that of the traditional serpentine channel at different flow rates.

4.1.2 Analysis of Temperature Uniformity Coefficient

The temperature uniformity coefficient is an important reference for assessing the temperature uniformity of the liquid cooling plate. As shown in Figure 9, the highest temperatures of the two flow channels under various operating conditions were obtained through simulation, and Figure 10 presents the results calculated using the temperature uniformity formula:

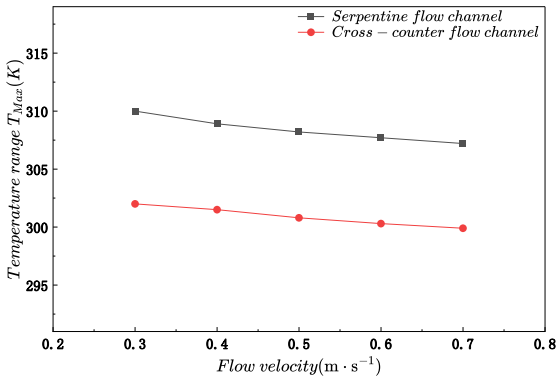

Fig.9: Line graph of maximum temperature for the two flow channels

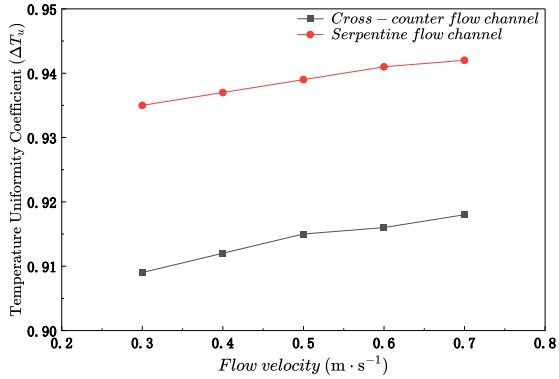

Fig.10: Temperature uniformity coefficient of the two flow channels

The temperature uniformity coefficient ΔTu of the cross-counter flow channel stabilizes in the range of 0.935 to 0.942, compared to 0.909 to 0.918 for the traditional serpentine channel, with an average increase of 0.025. Therefore, it can be considered that the cross-counter flow channel has better temperature uniformity compared to the traditional serpentine channel.

4.1.3 Performance Comparison of the Two Flow Channels

Temperature difference is a key indicator for evaluating the uniformity of the surface temperature distribution of a liquid-cooled plate, as it directly reflects its thermal management capability. The figure below shows a bar comparison of the temperature differences in cross-counter flow channels.

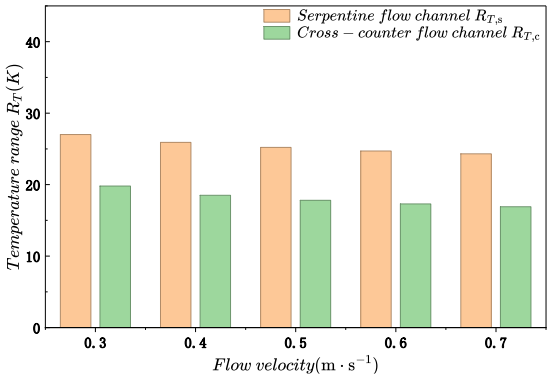

Fig.11: Bar chart of temperature range for the two flow channels

As shown in Figure 11, under all flow rate conditions, the temperature difference $R_{T,C}$ of the cross-counter flow channel is significantly lower than the $R_{T,S}$ of the serpentine channel. Taking a flow rate of 0.3 m/s as an example, $R_{T,C}$ is 7.2 K lower than $R_{T,S}$, with a reduction of 26.7%; even when the flow rate increases to 0.7 m/s, $R_{T,C}$ remains 7.5 K lower than $R_{T,S}$, a decrease of 30.9%. This result indicates that the local overheating problem significantly enhances temperature uniformity and resistance to local overheating.

4.2 Analysis of Pressure Drop Characteristics

4.2.1 Analysis of the Static Pressure Contour of Two Types of Liquid Cooling Plates

The static pressure contour map can visually display the distribution of static pressure inside the liquid-cooled plate flow channel, clearly reflecting the pressure level and attenuation trend through color changes.It can not only qualitatively judge the overall pressure drop, but also accurately identify the sources of resistance along the way and local resistance. It is an important basis for analyzing the pressure drop characteristics of liquid cooling plate, optimizing the channel structure, and improving the heat dissipation and flow performance.

As shown in Figure 12, the static pressure contour of the traditional serpentine channel shows a uniform gradient attenuation along the static pressure, and the color smoothly transitions from the dark red at the inlet to the dark blue at the outlet.This shows that the pressure drop mainly comes from the friction loss along the way, while the local loss at the U-bend is relatively small.The advantages of this design are uniform flow field and stable flow distribution, but the disadvantages are high total pressure drop.

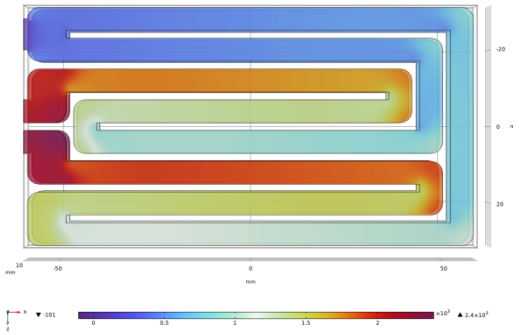

Fig.12: Static pressure contour of cross-counter flow channel

Figure 13 depicts the static pressure contour map of the cross-counter flow channel. Its total pressure drop (approximately 2.4×10^3 Pa) is notably lower than that of the traditional serpentine channel, directly reducing the driving power requirement of the circulating pump. By repeatedly changing the fluid flow direction within a limited space, the cross-counter flow channel achieves higher space utilization, making the overall structure of the liquid-cooled plate more compact within the same plate size. It is suitable

for integration scenarios with limited space and exhibits strong heat transfer performance.

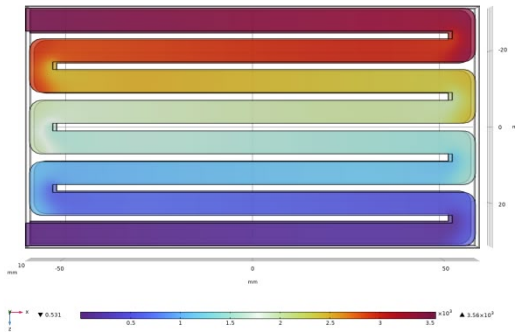

Fig.13: Static pressure contour of serpentine flow channel

4.2.2 Comprehensive comparison of pressure drop between two kinds of liquid cooling plates

In the liquid-cooled plate channel system, the pressure drop is positively correlated with the flow resistance. The pressure drop is the core physical parameter for quantifying the magnitude of flow resistance within the channel, and its value equals the total pressure difference between the channel inlet and outlet. Therefore, a comparative analysis of the pressure drop characteristics of serpentine channels and cross-counter flow channels under different flow rates is conducted.

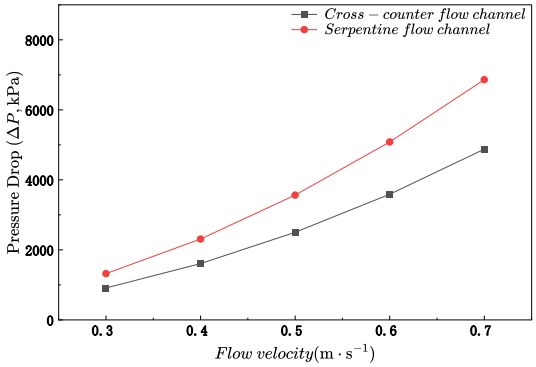

Fig.14: Line graph of pressure drop for the two flow channels

As shown in Figure 14, the pressure drop of cross counter current channel and traditional serpentine channel increases with the increase of flow rate, and the traditional serpentine channel has a faster lifting speed. When the flow rate is 0.3m/s, the pressure drop of serpentine channel and cross counter current channel is about 0.9kPa and 1.3kPa respectively; When the flow rate increases to 0.7m/s, the pressure drop increases to about 4.9kPa and 6.9kPa, respectively. The pressure drop in the cross counter current channel is about 41% higher than that in the traditional serpentine channel.

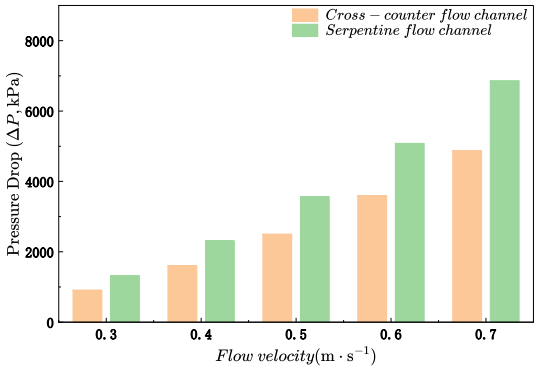

Fig.15: Bar chart of pressure drop for the two flow channels

As shown in Figure 15, the pressure drop of the cross counter current channel is higher than that of the serpentine channel in the speed range, so it can be concluded that the cross counter current channel has lower flow resistance, which can effectively reduce the driving power demand of the circulating pump, and reduce the system energy consumption and operation cost.

V. CONCLUSION

For the cross counter flow channel cold plate proposed in this study, the influence of channel velocity on pressure loss and cooling effect was studied:

(1) In terms of pressure drop characteristics, the growth rate of pressure drop in the serpentine channel is significantly faster than that in the cross counter current channel, and in the five groups of flow rates, the pressure drop in the serpentine counter current channel is higher than that in the cross counter current channel, with an average increase of 42.6%. Therefore, it can be seen that the flow resistance of cross counter current channel is significantly less than that of traditional serpentine channel.

(2) In terms of temperature uniformity, the temperature range of the cross counter current channel is significantly lower than that of the traditional serpentine channel under all flow rates. Taking the flow rate of 0.1m/s as an example, RT and s are 7.2K lower than R_T and C, with a decrease of 26.7%. Even at the flow rate of 0.7m/s, R_T and s are 7.5K lower than R_T and C, with a decrease of 30.9%, indicating that the cross counter current channel is superior to the traditional serpentine channel in temperature uniformity and local hot spot resistance.

In general, the cross counter current channel shows lower flow resistance in pressure drop characteristics, and

has more obvious advantages in temperature uniformity, which can effectively suppress the temperature difference inside the battery pack and improve the reliability and safety of the cooling system.

ACKNOWLEDGEMENTS

This work was supported by the Research Funding of GDUPT, Research on Heat Transfer Enhancement of Heat Sink by Inverse Calculation Design Method (No. 2019rc074) and Research on Intelligent Monitoring and Control Technology of Air Conditioning Noise Based on Quantitative Conjugate Gradient Method. Guangdong College Students' Innovation and Entrepreneurship Program in 2025, (Project No.: 25A015).

REFERENCES

[1] YAN H C, ZHANG X L. Heat dissipation performance of battery cooling system with composite phase change and air [J]. Cryogenics and Superconductivity, 2021, 49(12): 58-64.

[2] LAO Y L. Design and simulation analysis of liquid cooling structure for lithium battery [J]. Cryogenics and Superconductivity, 2021, 49(04): 78-84.

[3] Choudhari V G, Dhoble A S, Panchal S, et al. [J]. Journal of Energy Storage, 2021, 43: 103234.

[4] Luo J, Zou D Q, Wang Y S, et al. [J]. Chemical Engineering Journal, 2022, 430: 132741.

[5] Zhuang W C, Liu Z T, Su H Y, et al. [J]. Applied Thermal Engineering, 2021, 189: 116767.

[6] ZHANG H, ZHAO J, ZHANG Y D, et al. Study on the characteristics of intercooling plate for automotive power lithium battery cells [J]. Machinery Design & Manufacture, 2023, (06): 234-238+243.

[7] WU Z Z, TIAN L T, LIU J Z. Experimental study on liquid cooling thermal management of cylindrical lithium batteries [J]. Cryogenics and Superconductivity, 2022, 50(02): 42-48.

[8] Xie J, Ge Z, Zang M, et al. Structural optimization of lithium-ion battery pack with forced air cooling system [J]. Applied Thermal Engineering, 2017, 126: 583-593.

[9] Rao Z, Qian Z, Kuang Y, et al. Thermal performance of liquid cooling based thermal management system for cylindrical lithium-ion battery module with variable contact surface [J]. Applied Thermal Engineering, 2017, 123: 1514-1522.

[10] Karimi G, Azizi M, Babapoor A. Experimental study of a cylindrical lithium ion battery thermal management using phase change material composites [J]. Journal of Energy Storage, 2016, 8: 168-174.

[11] Zhao R, Gu J, Liu J. Optimization of a phase change material based internal cooling system for cylindrical Li-ion battery pack and a hybrid cooling design [J]. Energy, 2017, 135: 511-522.

[12] Shah K, Mckee C, Chalise D, et al. Experimental and numerical investigation of core cooling of Li-ion cells using heat pipes [J]. Energy, 2016, 113: 852-860.

[13] BERNARDI D, PAWLIKOWSKI E, NEWMAN J. A general energy balance for battery systems [J]. Journal of the Electrochemical Society, 1985, 132(1): 5-12.